Available online at www.sciencedirect.com
ScienceDirect
Journal of Sound and Vibration 310 (2008) 541–557
JOURNAL OF SOUND AND VIBRATION
www.elsevier.com/locate/jsvi

Destabilization of deep-water risers by a heaving platform

G.L. Kuiper[a,*], J. Brugmans[b], A.V. Metrikine[a]

[a]*Faculty of Civil Engineering and Geosciences, Delft University of Technology, Stevinweg 1, 2628 CN Delft, The Netherlands*
[b]*INTEC Engineering, Poortweg 14, 2612 PA Delft, The Netherlands*

Accepted 15 May 2007
The peer review of this article was organised by the Guest Editor
Available online 27 June 2007

Abstract

Offshore gas and oil fields are being discovered and exploited nowadays in water depths of more than 2000 m. In order to convey the hydrocarbon to the sea level, a steel slender pipe is installed between wellhead at the sea bed and floating platform. If used in deep waters, these pipes are commonly referred to as deep-water risers. The heave (vertical motion) of a floating platform induces a fluctuation in time of the axial tension of the riser. A possible and undesirable phenomenon is the excitation of a transverse riser vibration caused by this fluctuation. Owing to this fluctuation, the governing equation of transverse motion of the riser is a nonlinear partial differential equation containing a time-dependent coefficient. As a first step, this equation is linearized around the straight equilibrium, and stability of this equilibrium is investigated using the Galerkin method and the Floquet theory. Then, the dynamic equilibrium is studied that the riser reaches if its straight equilibrium is unstable. This is done using a numerical time-domain technique. Two qualitatively different mechanisms of stability loss are distinguished, discussed and exemplified. The first is classical parametric resonance that occurs solely due to periodic time variation of the axial tension. The second mechanism occurs if the amplitude of vibration of the platform is large enough to change tension into compression in a segment of the riser for a part of the vibration cycle. It is shown that the second mechanism can cause dangerously large dynamic stresses in the riser.

1. Introduction

Exploitation of offshore oil and gas fields is moving into deeper waters. In the last few years drilling activities took place in water depths of more than 2000 m, and it is expected that this is not the limit, since fields in 3000 m have already been discovered. In order to convey the hydrocarbon to the sea level, a steel pipe, conventionally referred to as a riser, is installed between wellhead at the sea bed and floating platform. A straight, top tensioned riser or a catenary-shape riser may be used, depending on the floating unit from which the riser is suspended.

Despite a number of advantages of the straight top-tensioned riser over the catenary riser, straight production risers have not been used yet in water depths over 2000 m. There are two specific concerns that stop the offshore industry from using top-tensioned straight risers in deep waters. The first concern is associated

*Corresponding author. Tel.: +31 15 2784671; fax: +31 15 2785767.
E-mail address: G.L.Kuiper@tudelft.nl (G.L. Kuiper).

0022-460X/$ - see front matter © 2007 Elsevier Ltd. All rights reserved.
doi:10.1016/j.jsv.2007.05.020

with fluctuation of the axial tension in the riser that is caused by vertical motion (heave) of the platform in waves. Although this fluctuation is significantly reduced by heave compensators, through which the riser is connected to the platform, it can be dangerous. The danger is that the fluctuating tension might destabilize the straight equilibrium of the riser and cause it to vibrate at a dangerously high level. The second concern is that the stroke of the heave compensator cannot always be made sufficiently large. This, however, can be dealt with by properly tuning the stiffness of the heave compensator to the environmental conditions.

This paper addresses the first above-mentioned concern, which is the possible destabilization of the riser due to fluctuation of the axial tension. The aim of the paper is to find the range of practically relevant amplitudes and frequencies of the vertical vibration of the platform, which may destabilize the riser and cause significant transverse vibrations. The second main aim is to discover possible mechanisms of the destabilization and to distinguish those mechanisms, which may lead to dangerously high dynamic amplification of the stresses in the riser.

Instability of a riser that is caused by fluctuation of its tension in time belongs to the class of parametric instabilities. This type of instability of offshore cables, risers and tethers received close attention of researchers in the past. Hsu [1] was one of the first who analysed parametric resonance for offshore cable applications. Patel and Park [2,3] studied dynamic behaviour of buoyant platform tethers assuming a constant pre-tension over the height and considering combined lateral and axial excitation at the top. The partial differential equation, governing the transverse motion of a tether, was reduced by them to a set of Mathieu equations with the help of the Galerkin method. These equations were then solved numerically taking into account the first four modes. In the first step of the analysis, determining the stability of the equilibrium, they did not consider the coupling between the modes. For a submerged cable of 1000 m length, parametrically excited at the top, Chatjigeorgiou and Mavrakos [4] studied numerically the transverse motion of the cable based on the first four modes taking the coupling between these modes into account. Suzuki et al. [5] performed a small-scale test in air with a Tefron tube of 11 m long that was parametrically excited at the top. They simulated dynamic behaviour of a 3000 m long free hanging riser, demonstrating the possible danger of parametric instability. Chatjigeorgiou and Mavrakos [6] found after extensive mathematical manipulations a closed-form solution for a parametrically excited riser based on the first two modes. These analytical limitations were the reason for Park and Jung [7] to use a finite element method for investigating long slender marine structures.

Parametric instability of straight deep-water cables, tethers and risers should be studied in two steps. First, stability of the straight equilibrium should be analysed by linearizing the equations of motion in the vicinity of this equilibrium. This allows determining the amplitude and frequency of parametric excitation which makes the straight equilibrium unstable. Then, the dynamic equilibrium should be studied, which the structure would reach if its straight equilibrium is unstable. At this stage, at least one of the two major nonlinearities that are capable of limiting structural vibrations should be accounted for. These nonlinearities are the geometric nonlinearity of the structure and hydrodynamic drag. Once the dynamic equilibrium is found, the corresponding displacements of and stresses in the structure can be found. On that basis a conclusion can to be drawn as to whether the parametric instability may cause a dangerously high level of vibration or not.

The first step of analysis, i.e. determination of stability of the straight equilibrium, is of major importance. It allows determining the parameter domain, in which a nonlinear analysis of the dynamic equilibrium is necessary. A notable problem at this stage is linearization of hydrodynamic damping, which is conventionally described as a quadratic function of the velocity of structural motion through surrounding water. Because of its quadratic character, in all above-mentioned papers the damping was not accounted for in the linear analysis of stability of the straight equilibrium. In this paper, based on recent results of Kuiper et al. [8], an improved description of hydrodynamic drag is used, which contains a linear term. Taking this term into account, the domain of parameters corresponding to unstable straight equilibrium is significantly reduced, which makes the nonlinear analysis of dynamic equilibrium significantly quicker. There are two more factors which have to be accounted for in stability analysis of the straight equilibrium. These are the depth-dependent axial tension and a high modal density of vibrations of deep-water risers. Both these factors make analytical analysis of stability of the straight equilibrium practically impossible. Therefore, instead of simplified analytical estimation of the equilibrium stability, which was used in the vast majority of papers on the subject, a numerical technique based on the Floquet theory [9] is applied here.

Another original component of this paper is an attempt to distinguish a number of qualitatively different mechanisms of stability loss by the riser. The difference between these mechanisms originates from the depth-dependent axial tension of the riser, which decreases significantly with the depth. This enables a so-called local dynamic buckling, which occurs if tension changes into compression in a segment of the riser during a part of the vibration cycle.

This paper is structured as follows. First, in Section 2, modelling assumptions are presented and discussed and an equation of motion for planar vibration of a top-tensioned deep-water riser is formulated. In Section 3, stability of the straight equilibrium is investigated employing the Floquet theory. Section 4 is devoted to analysis of the dynamic equilibrium in which the riser vibrates if its straight equilibrium is unstable. The mechanisms of stability loss are also discussed and exemplified in this section. The paper is finalized by a short discussion of the bending stress in the riser.

2. Assumptions and equation of motion

The top-tensioned riser under consideration is an initially straight, tensioned pipe of a finite length, as sketched in Fig. 1. It is assumed that the riser moves only in the plane of this figure. The transverse motion of the pipe is considered to be small and of a long wavelength relative to the diameter of the pipe so that the Euler–Bernoulli theory is applicable for description of the pipe dynamic bending.

The top of the riser is connected to the floating platform by means of a heave compensator, which has two functions. First, this device provides a large static tensile force at the top of the riser to avoid buckling. Secondly, it reduces the longitudinal stress variation induced by the relative vertical motion of the platform and the riser. As commonly done, the heave compensator is modelled in this paper as a pretensioned vertical spring with a stiffness that is much lower than the axial stiffness of the riser. At the bottom, the connection between the riser and the wellhead is modelled by a hinge.

Given the low stiffness of the heave compensator, the extensibility of the riser plays a minor role in its dynamics. Therefore, the riser is assumed to be inextensible so that any variation of tension at the top of the riser, imposed by the heave compensator, causes the corresponding instant change of tension all over the riser length.

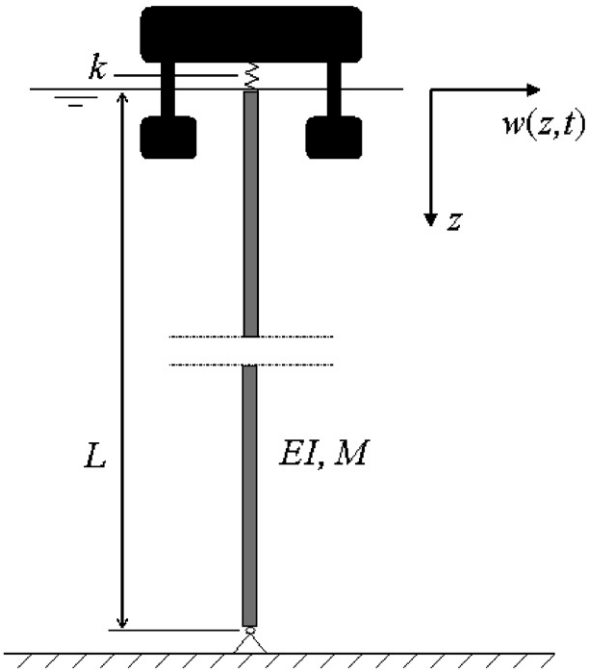

Fig. 1. Sketch of a deep-water riser connected to a floating platform.

With these assumptions, the equation of motion governing the transverse displacement $w(z,t)$ of the riser from its straight vertical equilibrium as a function of depth z and time t can be written as

$$EI\frac{\partial^4 w}{\partial z^4}-\frac{\partial}{\partial z}\left(T_e(z,t)\frac{\partial w}{\partial z}\right)+M\frac{\partial^2 w}{\partial t^2}+\mu A_1\frac{\partial w}{\partial t}+\frac{1}{2}\rho_f D_o A_2\left|\frac{\partial w}{\partial t}\right|\frac{\partial w}{\partial t}=0, \tag{1}$$

where EI is the bending stiffness of the pipe, T_e is the effective tension in the riser, M is the mass per unit length of the system (riser with internal fluid and added mass), μ is the dynamic viscosity of water around the riser, ρ_f is the water density, D_o is the outer diameter of the riser and A_1 and A_2 are two dimensionless constants. The last two terms on the left-hand side of Eq. (1) represent the hydrodynamic damping due to the surrounding water as explained in Kuiper et al. [8]. The term proportional to the transverse velocity of the pipe represents the viscous effects apparent in a thin boundary layer attached to the pipe. This term is important for small ($w/D_o<0.05/\pi$) displacements of the riser, and hence, for the onset of instability. For larger displacements and velocities the flow separates from the pipe, forming a turbulent wake behind it. In this regime the drag is proportional to the square of the pipe velocity. The constants A_1 and A_2 can be derived from experiments as shown in Kuiper et al. [8], assuming that the riser is surrounded by quiescent water. Conventionally, the measured hydrodynamic drag is expressed as a function of displacement amplitude and period of vibration. The idea in Ref. [8] is to reconstruct a time domain drag expression on the basis of the measured drag. To this end, the predictions obtained using the frequency and time domain descriptions are compared to each other requiring that displacement amplitudes are equal for the same external force. The coefficients A_1 and A_2 are identified by minimizing the differences between the predictions.

The additional forces associated with a flow through the riser [10] are neglected assuming that the flow is sufficiently slow.

The effective tension in the riser has static and dynamic components. The static component of the tension results from the pretension imposed by the heave compensator and submerged weight. In the offshore industry it is common practice to use a pretension that is 1.3 times higher than the submerged weight of the riser. The dynamic component of the tension is caused by the heaving platform. Owing to the assumption of inextensibility, this tension component depends only on time. Assuming that the platform vibrates harmonically, the effective tension can be expressed as

$$T_e(z,t)=W_a(-z+fL)-ka\,\sin(\Omega t), \tag{2}$$

where W_a is the submerged weight of the riser per unit length, f is a dimensionless pretension factor (in this paper, $f=1.3$), L is the length of the riser, k is the stiffness of the heave compensator, a and Ω are the amplitude and frequency of platform heave.

The boundary conditions at the ends of the riser, assuming that the connection of the heave compensator to the riser can be modelled as a hinge, are given as

$$w(0,t)=w(L,t)=0,\quad \left.\frac{\partial^2 w(z,t)}{\partial z^2}\right|_{z=0}=\left.\frac{\partial^2 w(z,t)}{\partial z^2}\right|_{z=L}=0. \tag{3}$$

Zero transverse motion at the top of the riser assumes no surge (horizontal motion) of the platform. Note that a small surge would not affect the results of linear stability analysis and only marginally the nonlinear one. A large surge would cause an additional variation of the riser tension and, consequently, would alter the results of both linear and nonlinear analyses.

Using the following dimensionless variables and parameters:

$$\eta=w/L,\quad \xi=z/L,\quad \tau=t\sqrt{EI/M}/L^2,\quad \tilde{\Omega}=\Omega\sqrt{M/EI}L^2,\quad \alpha=W_aL^3/EI,$$
$$\kappa=kaL^2/EI,\quad \varsigma=\mu L^2/\sqrt{MEI},\quad \gamma=\rho_f D_oL/2M,$$

the equation of motion (upon substitution of Eq. (2)) and the boundary conditions are rewritten as

$$\frac{\partial^4\eta}{\partial\xi^4}-\alpha(f-\xi)\frac{\partial^2\eta}{\partial\xi^2}+\kappa\,\sin(\tilde{\Omega}\tau)\frac{\partial^2\eta}{\partial\xi^2}+\alpha\frac{\partial\eta}{\partial\xi}+\frac{\partial^2\eta}{\partial\tau^2}+\varsigma A_1\frac{\partial\eta}{\partial\tau}+\gamma A_2\left|\frac{\partial\eta}{\partial\tau}\right|\frac{\partial\eta}{\partial\tau}=0, \tag{4}$$

$$\eta(0,\tau)=\eta(1,\tau)=0,\quad \left.\frac{\partial^2\eta(\xi,\tau)}{\partial\xi^2}\right|_{\xi=0}=\left.\frac{\partial^2\eta(\xi,\tau)}{\partial\xi^2}\right|_{\xi=1}=0. \tag{5}$$

Analysis of Eqs. (4) and (5) is subdivided into two parts. In the next section, the nonlinearity in Eq. (4) is disregarded to determine the domain of system parameters which correspond to instability of the straight shape of the riser. Then, in Section 4, the development of this instability is studied taking the nonlinearity into account.

3. Stability of the straight shape

Stability of the straight shape of the riser is determined by the linearized ($A_2=0$) equation of motion. To find the instability domain in the space of system parameters, it is customary to employ the Galerkin method. This method allows decomposing the partial differential equation of motion of the riser into an infinite set of ordinary differential equations with respect to time. Owing to the third term in Eq. (4), the latter equations will have coefficients that depend on time periodically. This fact calls for application of the Floquet theory [9], which is a convenient method for determining system parameters that break the parameter space into "stability" and "instability" domains. If the system parameters belong to the former domain, the straight (and the only) equilibrium of the riser is stable. On the contrary, if the system parameters belong to the "instability domain", the straight equilibrium is unstable and, given an initial perturbation, the energy of vibration of the riser would grow in time until the hydrodynamic nonlinearity would bring the energy input and the energy loss in balance.

This section is structured as follows. First, the linearized equation of motion is decomposed into a set of linear differential equations with periodic in time coefficients. Then, the Floquet theory is shortly described and applied numerically. Finally, the resulting stability charts are plotted and discussed focusing on the underlying physical mechanisms of instability.

3.1. Galerkin decomposition of linearized equation of motion

According to the Galerkin method, solution to the linearized equation (4) is sought for in the form:

$$\eta(\xi,\tau)=\sum_{m=1}^{\infty}\phi_m(\xi)q_m(\tau), \tag{6}$$

where $q_m(\tau)$ are unknown time-dependent functions and $\phi_m(\xi)$ are space-dependent shape functions forming a complete orthogonal set. In this paper, $\phi_m(\xi)$ are chosen as the eigenfunctions of the following linear differential operator:

$$\mathscr{L}_\xi=\frac{\mathrm{d}^4}{\mathrm{d}\xi^4}-\alpha(f-\xi)\frac{\mathrm{d}^2}{\mathrm{d}\xi^2}+\alpha\frac{\mathrm{d}}{\mathrm{d}\xi} \tag{7}$$

satisfying the boundary conditions, Eq. (5). The corresponding eigenvalues λ_m are all imaginary and in the following are represented by the real-valued eigenfrequencies $\Omega_m=\mathrm{i}\lambda_m$. The eigenfrequencies and eigenfunctions of $\mathscr{L}_\xi$ can be found numerically or in a closed form using a power series expansion [11].

Substituting Eq. (6) into the linearized Eq. (4), multiplying through by $\phi_n(\xi)$, and integrating over $\xi\in(0,1)$, it is found that

$$\frac{\mathrm{d}^2q_n}{\mathrm{d}\tau^2}+\varsigma A_1\frac{\mathrm{d}q_n}{\mathrm{d}\tau}+\Omega_n^2q_n+\kappa\,\sin(\tilde{\Omega}\tau)\sum_{m=1}^{\infty}B_{mn}q_m=0,$$

$$B_{mn}=\int_0^1\frac{\mathrm{d}^2\phi_m}{\mathrm{d}\xi^2}\phi_n\,\mathrm{d}\xi\Big/\int_0^1\phi_n^2\,\mathrm{d}\xi,\quad n,m=1,2,\ldots,\infty. \tag{8}$$

This infinite set of ordinary differential equations can be approximated by a finite system of $2N$ first-order coupled equations:

$$\begin{cases} \dfrac{\mathrm{d}y_n}{\mathrm{d}\tau} = y_{N+n}, \\ \dfrac{\mathrm{d}y_{N+n}}{\mathrm{d}\tau} = -\varsigma A_1 y_{N+n} - \Omega_n^2 y_n - \kappa \sin(\tilde{\Omega}\tau) \sum\limits_{m=1}^{\infty} B_{mn} y_m, \quad n,m = 1,2,\ldots,N, \end{cases} \tag{9}$$

where n and N stand for, respectively, the mode number and the total number of modes considered. In matrix notation, Eq. (9) can be written as

$$\dot{\mathbf{y}} = \mathbf{A}(\tau)\mathbf{y}, \tag{10}$$

where $\mathbf{y} = [y_1, y_2, \ldots, y_{2N}]^{\mathrm{T}}$, the overdot means ordinary derivative with respect to τ, and $\mathbf{A}(\tau)$ is a $2N \times 2N$ matrix, which is periodic in time. i.e. $\mathbf{A}(\tau) = \mathbf{A}(\tau + 2\pi/\tilde{\Omega})$. Stability of the equilibrium of Eq. (10) can be studied employing the Floquet theory, which is briefly outlined in the next sub-section. A rigorous description of this theory can be found in Ref. [9].

3.2. Floquet theory

The Floquet theorem [12] states that the fundamental matrix solution $\mathbf{U}(\tau)$ of Eq. (10) is given as

$$\mathbf{U}(\tau) = \mathbf{P}(\tau)\exp(\tau\mathbf{F}), \tag{11}$$

where $\mathbf{P}(\tau)$ is a periodic $2N \times 2N$ matrix function with the period $T = 2\pi/\tilde{\Omega}$ and $\mathbf{F}$ is a $2N \times 2N$ matrix (possibly complex). As follows from Eq. (11), the fundamental matrix solution $\mathbf{U}(\tau)$ grows in time if and only if at least one of the eigenvalues of $\mathbf{F}$ has a positive real part.

To find the eigenvalues of $\mathbf{F}$ numerically, it is convenient to introduce the state transition matrix $\mathbf{\Phi}(\tau, \tau_0)$:

$$\mathbf{\Phi}(\tau, \tau_0) = \mathbf{U}(\tau)\mathbf{U}^{-1}(\tau_0). \tag{12}$$

Substituting the fundamental matrix solution into this expression and setting $\tau = T$, $\tau_0 = 0$, one obtains

$$\mathbf{\Phi}(T, 0) = \mathbf{P}(T)\exp(T\mathbf{F})\mathbf{P}^{-1}(0) = \mathbf{P}(0)\exp(T\mathbf{F})\mathbf{P}^{-1}(0). \tag{13}$$

Stability of linear systems and, in particular, matrix $\mathbf{F}$ is independent of initial conditions. Therefore, any initial conditions can be employed in numerical evaluation of $\mathbf{F}$. As can be seen from Eq. (13), it is convenient to choose initial conditions such that $\mathbf{U}(0) = \mathbf{P}(0) = \mathbf{I}$, where $\mathbf{I}$ is the identity matrix. In this case, Eq. (13) reduces to

$$\mathbf{\Phi}(T, 0) = \exp(T\mathbf{F}). \tag{14}$$

Therefore, with the initial conditions $\mathbf{U}(0) = \mathbf{P}(0) = \mathbf{I}$, matrix $\mathbf{F}$ can be expressed through the state transition matrix over the period T:

$$\mathbf{F} = T^{-1} \ln(\mathbf{\Phi}(T, 0)). \tag{15}$$

The state transition matrix $\mathbf{\Phi}(T, 0)$ can be found by solving numerically Eq. (10) in the time interval $0 \leqslant \tau \leqslant T$. Eq. (10) has to be solved $2N$ times, each time giving one of the components of the vector $\mathbf{y}$ the unit initial value, while keeping all other initial values zero. For example, to obtain the first row of the fundamental matrix solution, one should take $y_1(0) = 1$ and $y_i(0) = 0, \quad i = 2,3,\ldots,2N$; the second row is obtained by taking $y_2(0) = 1$ and $y_i(0) = 0, \quad i = 1,3,4,\ldots,2N$ and so forth.

Once the state transition matrix $\mathbf{\Phi}(T, 0)$ is composed, the eigenvalues $\lambda_i, \quad i = 1,2,\ldots,2N$ of this matrix have to be found. According to Eqs. (14) and (15), if the absolute value of λ_i is larger than one, the corresponding eigenvalue of matrix $\mathbf{F}$ has a positive real part. Therefore, a system governed by Eq. (10) is stable if the absolute value of all eigenvalues of $\mathbf{\Phi}(T, 0)$ is not larger than one:

$$|\lambda_i| \leqslant 1, \quad i = 1,2,\ldots,2N. \tag{16}$$

Correspondingly, at the boundary of the stability zone in the space of the system parameters the absolute value of at least one of these eigenvalues equals one, whereas the absolute values of all other eigenvalues are not larger than one. This criterion is applied in the next sub-section to find the instability zones of the riser on the basis of Eq. (9).

3.3. Stability of the straight equilibrium

Stability of the straight equilibrium of the riser is studied in the plane of the frequency and amplitude of the harmonic heave motion of the platform. The frequency Ω is varied between 0.1 and 2.2 rad/s, whereas the amplitude a is varied between 0.0 and 5.0 m. In the chosen frequency range, sea waves contain the most energy.

The other parameters of the system are chosen as follows. The stiffness k of the heave compensator in practice is commonly tuned to compensate for the submerged weight of the riser in case that the platform heaves with a given critical amplitude a_c, usually set at 10 m. This means that a realistic value of k is given as

$$k = LW_a/a_c. \tag{17}$$

Further in this section the stiffness of the heave compensator will be varied to investigate its effect on stability of the riser.

Kuiper et al. [8] estimated the coefficient A_1 at 27.0×10^3 (this coefficient indicates the amount of linear viscous fluid damping). This estimation was based on experiments with the Stokes parameter being around 10^6. The Stokes parameter is defined as $\beta = D_o^2/(\upsilon T)$, where T is the period of oscillation and υ is the kinematic viscosity of water. Since the Stokes parameter for the deep-water riser that is considered in this paper is in the order of 10^3–10^4, depending on the mode of vibration, a lower value of A_1 is to be expected. Besides, the outer wall roughness of the riser influences the value of A_1. To cope with these uncertainties, three values of A_1 are considered, namely 6.75×10^3, 13.5×10^3 and 27.0×10^3. The values of the other parameters are shown in Table 1.

Fig. 2 shows stability charts for the three damping coefficients A_1. The dotted domains correspond to unstable behaviour of the riser. The stability charts have been computed by considering the first 10 modes ($N = 10$). With the chosen parameters (see Table 1), the first natural frequency is 0.137 rad/s, whereas the tenth is 1.38 rad/s. The relatively wide distinct instability zones in Fig. 2 correspond to the first-order parametric resonance, for which the relation $\Omega = 2\omega_n$ holds (ω_n is the nth natural frequency of the riser). The positions of these zones are specified in the top left chart of Fig. 2. The narrower zones are related to either combined or higher order parametric resonance conditions. Comparing the three stability charts in Fig. 2, it can be concluded that the instability zones shrink, if the linear viscous damping is increased. The distinct first-order parametric zones disappear for sufficiently large linear viscous damping. In the absence of damping the instability zones would begin at the horizontal axis. Besides, many more very narrow instability zones associated with higher order and combined parametric resonance would appear.

From a practical viewpoint it is interesting to investigate the effect of the stiffness of the heave compensator on the riser stability. Fig. 3 presents three stability charts obtained for three values of this stiffness. This figure shows that the stiffness of the heave compensator influences stability of the riser dramatically. The higher the stiffness, the larger the instability zone in the chosen practically relevant parameter domain. Therefore, though

Table 1
Values of the system parameters used in calculations

Parameters			
E	2.1×10^{11} N/m^2	ρ_f	1.025×10^3 kg/m^3
L	2000 m	μ	1.00×10^{-3} kg/m/s
D_o	0.25 m	M	136.7 kg/m
D_i	0.22 m	W_a	735.3 N/m
f	1.3	A_2	0.24
a_c	10 m		

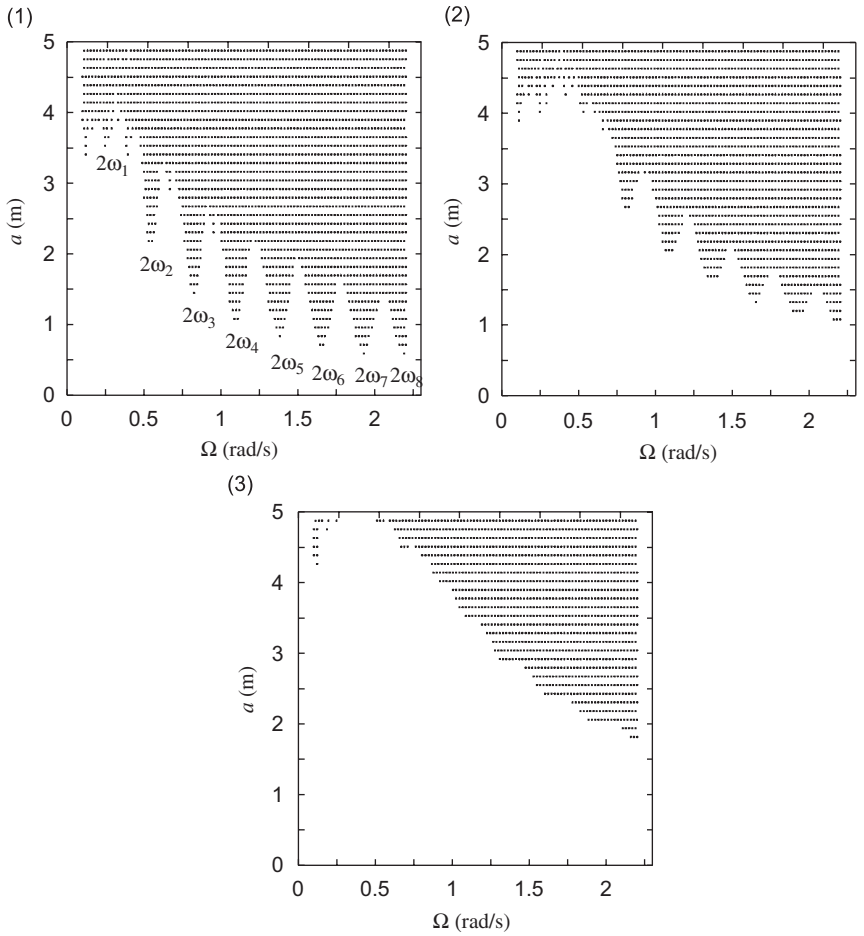

Fig. 2. Stability charts obtained from the linearized equation of motion with $k = LW_a/a_c$: (1) $A_1 = 6.75 \times 10^3$, (2) $A_1 = 13.5 \times 10^3$, and (3) $A_1 = 27.0 \times 10^3$.

a stiffer heave compensator is much easier to construct in practice, relatively soft heave compensators are recommended to ensure stability of the riser.

3.4. Preliminary discussion of the mechanisms of instability

Though the Floquet theory is a convenient tool for studying stability of the straight equilibrium of the riser, this theory does not enlighten in detail the physical mechanisms of this instability. It is clear, for example, that instability of the riser is not necessarily related to parametric resonance but also might be caused by local buckling of the riser. Indeed, the mean value of the tension of the riser decreases with the distance from the sea surface. Therefore, the platform, if heaving with sufficiently large amplitude, can change the tension into compression near the sea bottom. If the local compression cannot be counteracted by the restoring forces, the riser will lose stability. In order to check whether local buckling near the sea bottom might occur, a static analysis is carried out to compute the maximum platform set down beyond which the riser buckles. Neglecting the time dependent terms in Eq. (4) and considering the floating platform in the lowest position, i.e. when the riser top tension has its lowest value, the following equation governing static equilibrium of the riser can be deduced:

$$\frac{\partial^4 \eta}{\partial \xi^4} - (\alpha(f-\xi)-\kappa)\frac{\partial^2 \eta}{\partial \xi^2} + \alpha \frac{\partial \eta}{\partial \xi} = 0. \tag{18}$$

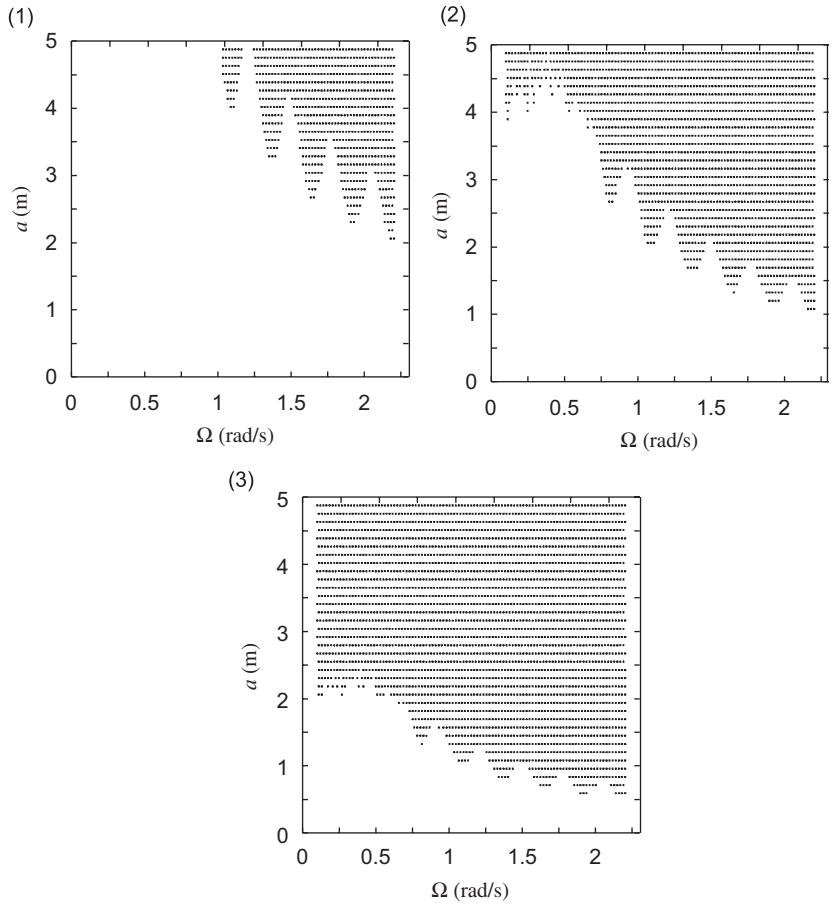

Fig. 3. Stability charts obtained from the linearized equation of motion for different spring constants of the heave compensator: (1) $k = LW_a/(2a_c)$, (2) $k = LW_a/a_c$, and (3) $k = 2LW_a/a_c$ for a linear damping coefficient of $A_1 = 13.5 \times 10^3$.

The general solution of this equation can be written in terms of the Airy functions of the first, $\mathrm{Ai}(\psi)$, and the second kind, $\mathrm{Bi}(\psi)$:

$$\eta(\xi) = C_1 + C_2 \int_0^{\xi} \mathrm{Bi}(\psi_1)\,\mathrm{d}\xi_1 + C_3 \int_0^{\xi} \mathrm{Ai}(\psi_1)\,\mathrm{d}\xi_1 + C_4 \int_0^{\xi} \left(-\mathrm{Ai}(\psi_1)\mathrm{Bi}(\psi_1) \int_0^{\xi_1} \mathrm{Bi}(\psi_2)\,\mathrm{d}\xi_2 \int_0^{\xi_1} \mathrm{Ai}(\psi_2)\,\mathrm{d}\xi_2 \right) \mathrm{d}\xi_1, \tag{19}$$

where $\psi_1 = (\alpha(f - \xi_1) - \kappa)/\alpha^{2/3}$and $\psi_2 = (\alpha(f - \xi_2) - \kappa)/\alpha^{2/3}$. Substituting Eq. (19) into the boundary conditions, Eq. (5), a system of four linear algebraic equations can be obtained with respect to the unknown constants C_1–C_4. Static instability occurs if the determinant of this system of equations equals zero. This determinant is studied numerically by gradually increasing the value of κ. The calculation shows that buckling will occur if $\kappa = 14.3$, which corresponds to a vertical set down of 3.14 m using parameters in Table 1 and $k = LW_a/a_c$. At first glance, it might seem remarkable that in Fig. 2 some areas are stable for amplitudes exceeding this value. However, it is known that parametric excitation can stabilize dynamical systems. For frequencies tending to zero, the instability boundary originates from the 'static buckling amplitude' of 3.14 m. It is not visible in Fig. 2 because the lowest frequency considered is 0.1 rad/s. The effect of local buckling is investigated in more detail in the next section.

4. Nonlinear analysis of instability development

If the straight shape of the riser is stable, any perturbation of this shape would slowly decay and the riser would return to its straight equilibrium. On the contrary, if the straight shape is unstable, any perturbation would lead to a temporary growth of the energy of transverse vibration of the riser. This growth would proceed until the energy loss caused by the nonlinear hydrodynamic damping would balance the energy input by the heaving platform, leading to a dynamic equilibrium. In this section, this dynamic equilibrium is studied numerically and conclusions are drawn as to different scenarios leading to this equilibrium.

4.1. Nonlinear time domain analysis of the dynamic equilibrium

To study the dynamic equilibrium that the riser reaches if its straight equilibrium is unstable, the original nonlinear equation of motion, Eq. (4), with the boundary conditions, Eq. (5), are discretized in space using a second-order central difference approximation. The following initial conditions are used:

$$\eta(\xi,0)=\hat{\eta}\,\sin(\xi\pi) \quad \text{and} \quad \left.\frac{\partial\eta(\xi,\tau)}{\partial\tau}\right|_{\tau=0}=0, \tag{20}$$

where $\hat{\eta}=0.01$. The length of the riser L is divided into S segments, all having a length of $h=L/S$. The first node is at $z=0$ and the $(S+1)$th node is at $z=L$. To incorporate the boundary conditions, at each end one dummy node is added. This discretization gives a system of $(S+1)$ second-order nonlinear ordinary differential equations with respect to time, or, equivalently, a system of $2(S+1)$ first-order ordinary differential equations. This latter system is solved numerically by using the Runga–Kutta–Verner fifth-order method.

Before giving results of numerical analysis, it is important to discuss the major physical limitation of Eq. (4). Though this equation is nonlinear, the only nonlinearity taken into account in this equation is related to the hydrodynamic drag. No geometrical nonlinearities are accounted for, which limits applicability of Eq. (4) to relatively small rotations and curvatures of the riser. Since the bending stiffness has minor effect on dynamics of deep-water risers, the major limitation to be concerned with is the rotation of the riser. The geometric nonlinearity related to large rotations can be neglected if $(\partial w/\partial z)^2 \ll 1$, which is the classical condition of small transverse vibrations of taut strings. In order to distinguish the domain in the parameter space, within which the condition of small inclinations is violated, the limit of $(\partial w/\partial z)^2=0.2$ was chosen. If during a numerical run this limit was exceeded, the run was interrupted and the resulting riser amplitude was set to 7.5 m. No physical significance is attached to this value, which is chosen to achieve good graphical representation of the results. The parameter domain that is distinguished by this value of riser amplitude needs additional analysis which takes geometric nonlinearities of the riser into account.

Employing the above described numerical approach, three-dimensional charts are obtained that are shown in Fig. 4(a–c). The horizontal axes in these figures show the frequency and heave amplitude of the platform, whereas the vertical axis gives the maximum deflection along the riser in the dynamic equilibrium. These charts are obtained using the same parameters as used in the three charts in Fig. 2.

An in-depth study of Fig. 4 and corresponding dynamic deflections of the riser allows distinguishing three qualitatively different scenarios leading to the dynamic equilibrium of the riser (the corresponding frequencies and amplitudes of the platform are indicated in Fig. 5). These scenarios can be referred to as

- classical parametric resonance (area 1 in Fig. 5);
- sub-critical local dynamic buckling (area 2 in Fig. 5);
- super-critical local dynamic buckling (area 3 in Fig. 5).

In the following sub-sections the specific features of each of these scenarios are discussed in detail.

4.2. Classical parametric resonance

The frequency and amplitude of the platform that correspond to destabilization of the riser via classical parametric resonance correspond to area 1 in Fig. 5. Subject to these frequencies and amplitudes of excitation,

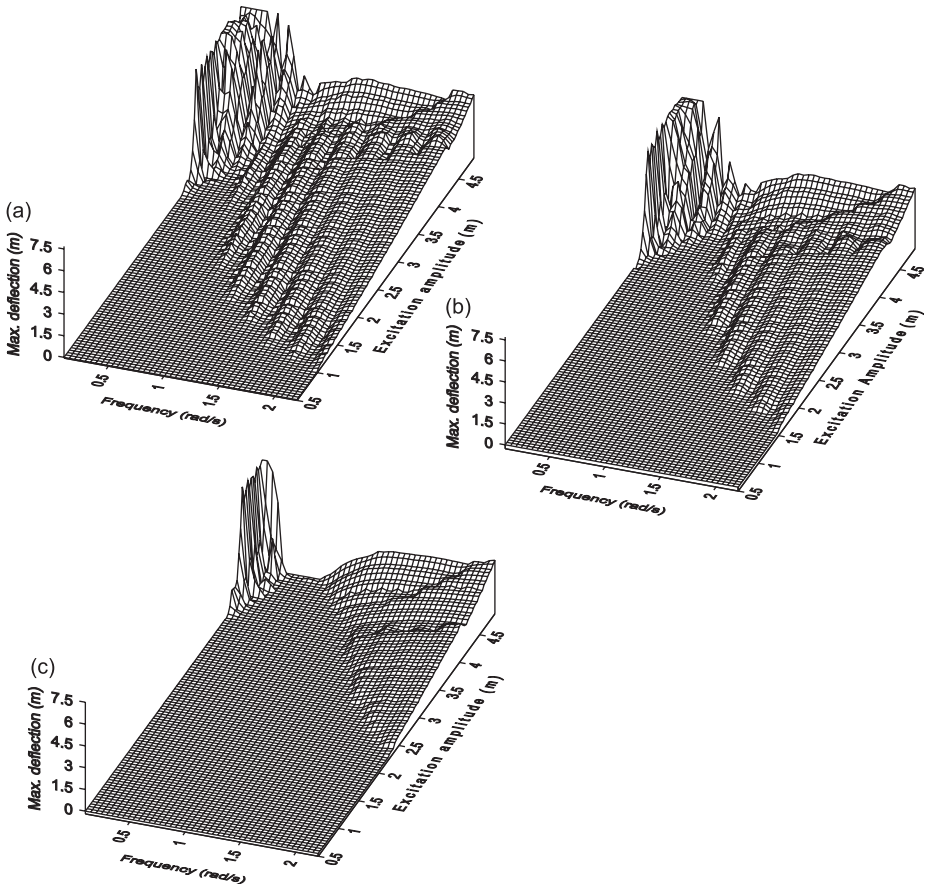

Fig. 4. Maximum deflection of the riser vs. the amplitude and frequency of the heaving platform for (a) $A_1 = 6.75 \times 10^3$, (b) $A_1 = 13.5 \times 10^3$, and (c) $A_1 = 27.0 \times 10^3$.

the riser gains energy (owing to simultaneous variation of tension) along its entire length and loses stability at a specific mode or a combination of modes.

As an example, a deep-water riser subjected to a platform that heaves with amplitude of 3.0 m and frequency of 1.6 rad/s is considered. This frequency can be shown to be about twice the sixth natural frequency of small vibrations of the riser. The deflection of the midpoint of the riser is depicted as a function of time in Fig. 6 starting from a moment when the influence of initial conditions has almost disappeared. This figure shows that, in accordance with the condition of the main zone of classical parametric resonance, the dominant frequency of vibration equals about half the excitation frequency. Correspondingly, in the dynamic equilibrium the riser vibrates primarily in its sixth mode, as can be seen in Fig. 7. Note that in this figure the influence of spatially varying tension is clearly visible. Due to the tension decrease with the distance from the sea surface, the amplitude of the riser increases with this distance, whereas the internodal spacing decreases.

4.3. Sub-critical local dynamic buckling

For frequencies and heave amplitudes of the platform corresponding to area 2 in Fig. 5, the riser experiences what can be called a 'sub-critical local dynamic buckling'. This type of instability occurs if the amplitude of the heaving platform is sufficiently large to change tension into compression at a segment of the riser during a part of the vibration period. The resulting compressive force should be large enough to overcome restoring forces and cause local buckling of the riser. This buckling occurs near the sea bottom because the tension of the riser

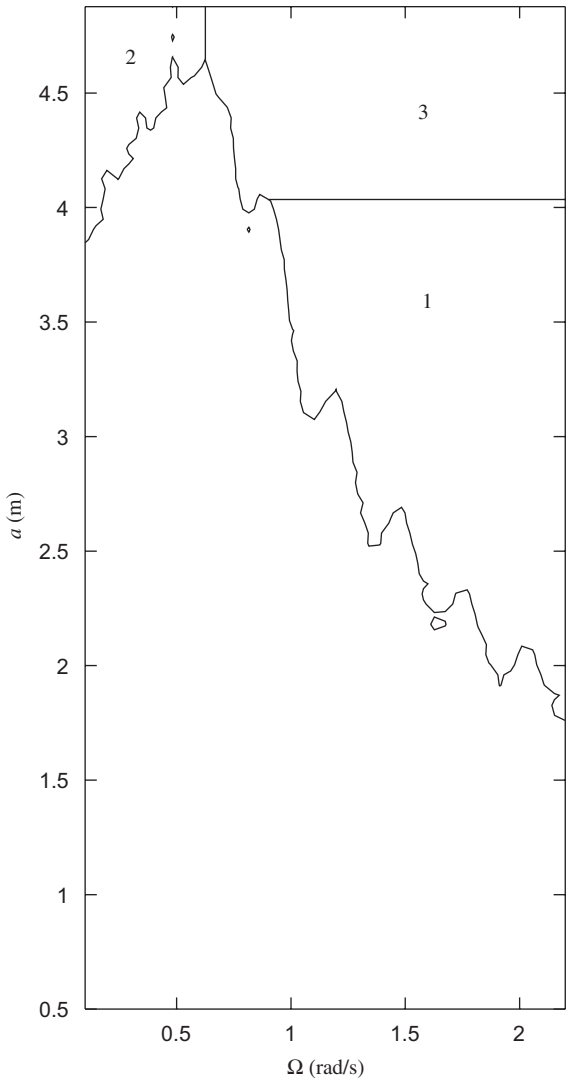

Fig. 5. Three areas of qualitatively different destabilization mechanisms of the riser ($A_1 = 13.5 \times 10^3$, $k = LW_a/a_c$).

is the smaller the closer the riser cross-section to the sea bottom. The time interval within which the buckling occurs is limited by the part of the vibration cycle that corresponds to a compressive force in the riser. During this time interval, the riser deflection grows locally and starts propagating along the riser. Then, the riser becomes tensioned again and the buckling-induced local disturbance propagates along the riser gaining no energy. In the regime of 'sub-critical local dynamic buckling', this disturbance is not amplified by the next local buckling that happens after one period of vibration but travels along the riser until vanishing due to hydrodynamic damping. Thus, in the regime under consideration a sequence of distinct deflection pulses travels along the riser. Obviously, in the case that the excitation frequency is low enough ($\Omega \leqslant 0.5$), these pulses do not amplify each other so that the buckling occurs not too often. Therefore, the area in Fig. 5 that corresponds to this regime occupies the region of relatively high amplitudes and low frequencies.

To exemplify the riser vibration in the case of sub-critical local dynamic buckling, the deflection of a riser point close to the sea bottom (at $z = 0.9L$) is shown in Fig. 8 as a function of time. The amplitude and the frequency of the platform vibration are, respectively, 4.5 m and 0.2 rad/s. Fig. 8 clearly shows a sequence of short pulses that pass through the chosen cross-section. These pulses are very similar to each other and occur

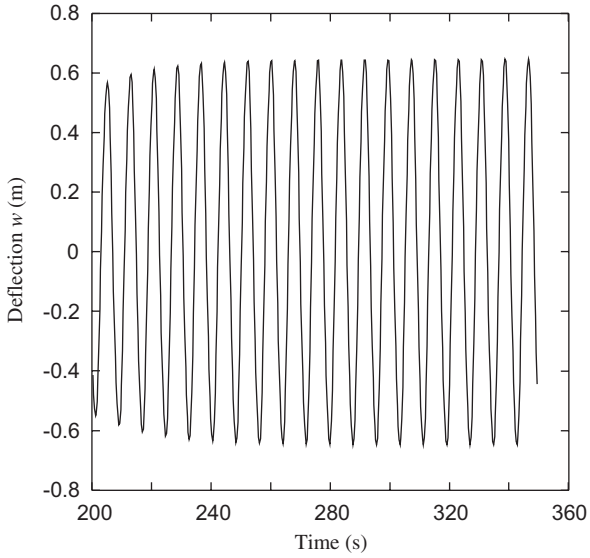

Fig. 6. Transverse deflection of the midpoint of the riser vs. time for $a = 3.0\,\text{m}$, $\Omega = 1.6\,\text{rad/s}$ ($A_1 = 13.5 \times 10^3$, $k = LW_a/a_c$).

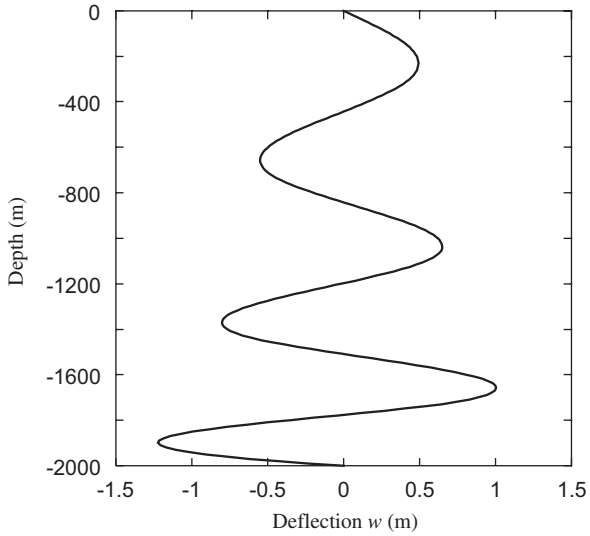

Fig. 7. Shape of the riser in the dynamic equilibrium for $a = 3.0\,\text{m}$, $\Omega = 1.6\,\text{rad/s}$ ($A_1 = 13.5 \times 10^3$, $k = LW_a/a_c$).

periodically. One can see that between the pulses the riser deflection is nearly zero, which implies that the pulses do not amplify each other.

Initiation and propagation of the pulses that result from sub-critical local dynamic buckling is illustrated in Fig. 9 that shows the shape of the riser at three successive instants. Fig. 9(a) shows local buckling near the sea bottom that results in a relatively large deflection of the riser. Figs. 9(b) and (c) show two successive instants when the riser is everywhere in tension and the deflection pulse excited by the buckling travels upward. While propagating, this pulse widens owing to dispersion and loses energy because of hydrodynamic damping. Upon reflection from the upper end of the riser, this pulse would travel downward but by the time it would reach the sea bottom its energy would be negligible and the contribution of this pulse to the riser deflection in the dynamic equilibrium would vanish.

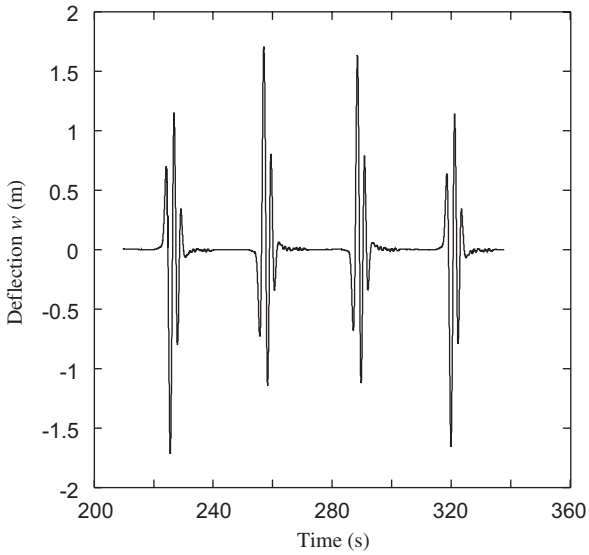

Fig. 8. Transverse deflection of a point of the riser at $z = 0.9L$ vs. time for $a = 4.5\,\text{m}$, $\Omega = 0.2\,\text{rad/s}$ ($A_1 = 13.5 \times 10^3$, $k = LW_a/a_c$).

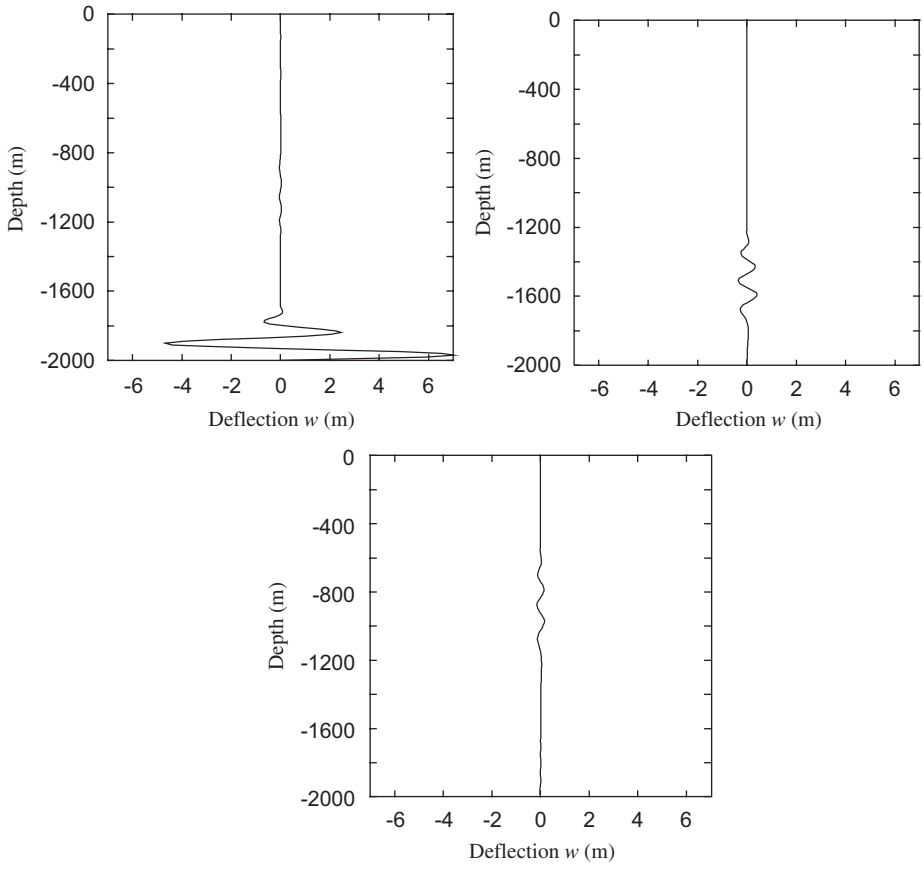

Fig. 9. Shape of the riser at three successive time moments for $a = 4.5\,\text{m}$, $\Omega = 0.2\,\text{rad/s}$ ($A_1 = 13.5 \times 10^3$, $k = LW_a/a_c$).

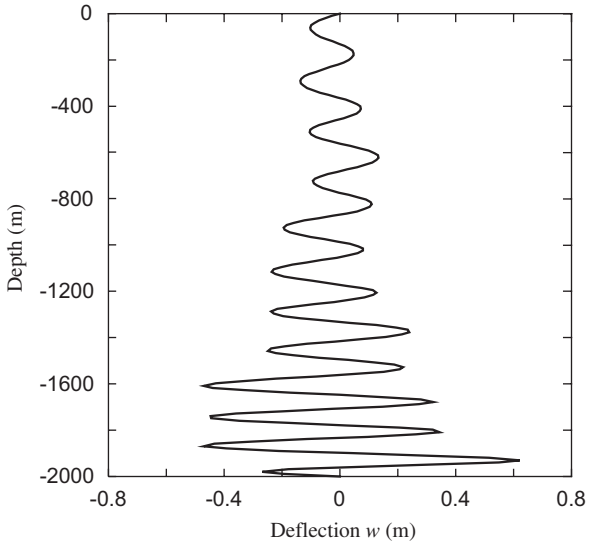

Fig. 10. Shape of the riser in the dynamic equilibrium for $a = 4.5\,\mathrm{m}$, $\Omega = 1.5\,\mathrm{rad/s}$ ($A_1 = 13.5 \times 10^3$, $k = LW_a/a_c$).

4.4. Super-critical local dynamic buckling

The main difference between the sub-critical and super-critical local dynamic buckling is the frequency of the buckling events. In the latter regime this frequency is larger so that the buckling-generated pulses are not separated in space as in the sub-critical case.

In the regime of super-critical local dynamic buckling, the amplitude and frequency of the heave of the platform correspond to area 3 in Fig. 5. Within this area both the amplitude and frequency are relatively high.

To exemplify this instability regime, the typical shape of the riser in dynamic equilibrium is shown in Fig. 10 for $a = 4.5\,\mathrm{m}$ and $\Omega = 1.5$ rad/s. Obviously, in contrast to the sub-critical regime, one cannot distinguish separate buckling-induced pulses. Instead, the riser vibrates in a certain combination of its modes. This vibration is reached, however, not via classical parametric resonance but via periodic generation of buckling-induced pulses near the bottom that is followed by decomposition of these pulses (due to dispersion) into a combination of riser modes.

The difference between the sub- and super-critical local dynamic buckling can also be clearly illustrated by phase plots, as shown in Fig. 11 for a point close to the sea bottom, $z = 0.9L$. The frequencies of vibration of the platform in the left and right plots are 0.2 and 1.5 rad/s, respectively. In both cases the heaving amplitude is 4.5 m. For sub-critical local dynamic buckling (the left figure) the phase trajectories first run away from the origin and then, quickly, return back to the vicinity of the origin where they stay for some time. This behaviour of the trajectories corresponds to generation of the pulse, its propagation away from the generation area and the "silent time" before the next buckling occurs. In the regime of super-critical local dynamic buckling (the right figure) the phase trajectories in the dynamic equilibrium do not approach the origin. This is because each new buckling-induced pulse is generated before the previous ones have been dissipated by the hydrodynamic damping.

5. Bending stresses in the riser

From the viewpoint of design of deep-water risers, it is more important to calculate stresses in the riser than its deflections. A heaving platform induces bending, axial and radial stresses in the riser. Here only the maximum bending stress in dynamic equilibrium is considered and compared to the yield stress of steel, which is around $3.8 \times 10^8\,\mathrm{N\,m^{-2}}$. The bending stress at the outer diameter is calculated using the

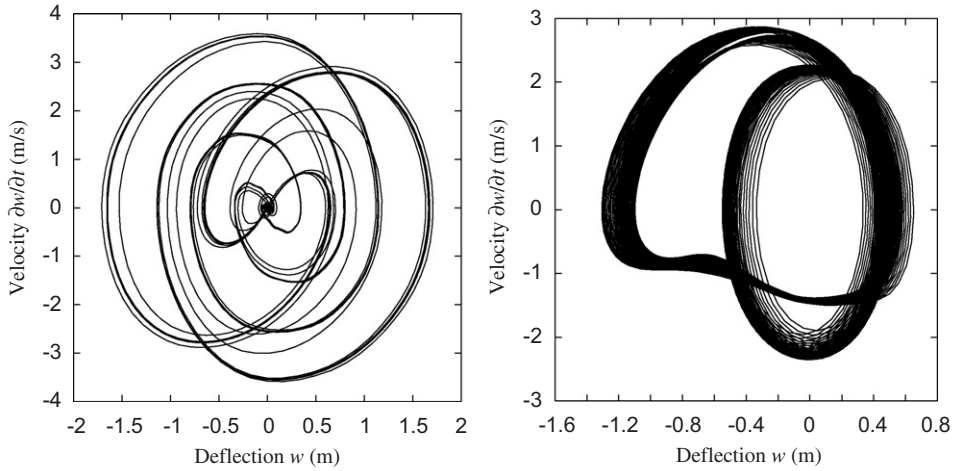

Fig. 11. Phase portraits of the riser motion at $z = 0.9L$ in case of sub-critical (left) and super-critical (right) local dynamic buckling ($A_1 = 13.5 \times 10^3$, $k = LW_a/a_c$).

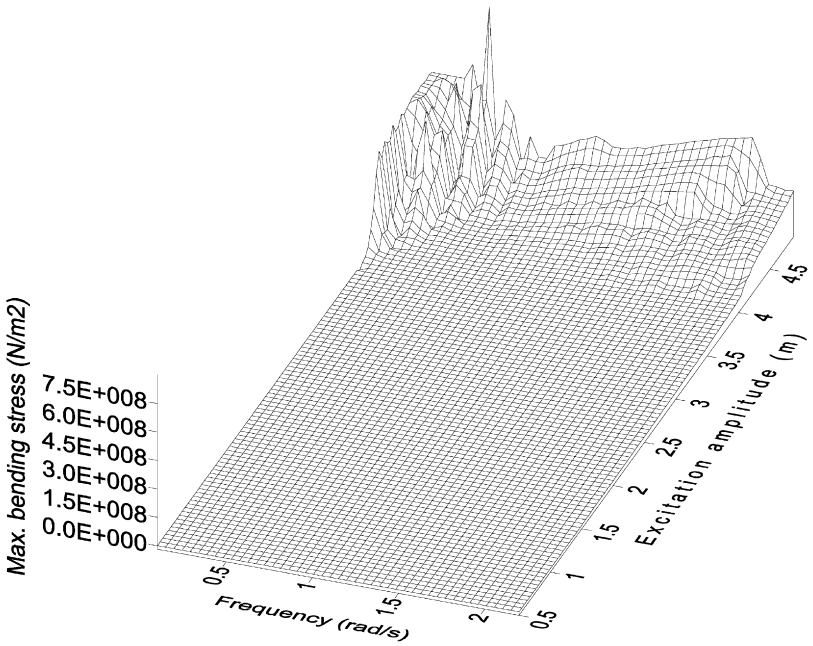

Fig. 12. Maximum bending stress in the riser vs. the amplitude and frequency of the heaving platform ($A_1 = 13.5 \times 10^3$, $k = LW_a/a_c$).

following equation:

$$\sigma_b(z) = E\frac{\partial^2 w(z)}{\partial z^2}\frac{D_o}{2}, \tag{21}$$

where $\sigma_b(z)$ is the bending stress and E is the elasticity modulus of steel. The same range of amplitudes and frequencies of vibration of the platform is considered as in the previous sections, i.e. $0.1\,\text{rad/s} \leqslant \Omega \leqslant 2.2\,\text{rad/s}$ and $0 \leqslant a \leqslant 5.0\,\text{m}$. As in the previous section, the calculations are interrupted if $(\partial w/\partial z)^2 > 0.2$ and in this case the maximum riser bending stress is put to $5.0 \times 10^8\,\text{N m}^{-2}$ (no physical significance is attached to this value). The bending stress is computed using parameters in Table 1, $k = LW_a/a_c$ and $A_1 = 13.5 \times 10^3$. The maximum bending stress along the riser, subjected to the chosen range of platform motions, is shown in Fig. 12. From this figure it can be concluded that classical parametric resonance (area 1 in Fig. 5) of the riser corresponds to

insignificant bending stress, while local dynamic buckling (areas 2 and 3 in Fig. 5) is a real threat for the riser, since the bending stress exceeds the yield stress.

6. Conclusion

In this paper, stability of a straight deep-water riser connected to a heaving floating platform has been considered. It is shown that a vertical harmonic motion of the platform can result in a loss of stability of the riser. Three distinct mechanisms of stability loss may occur, namely classical parametric resonance, sub-critical local dynamic buckling and super-critical local dynamic buckling. The two latter mechanisms are the most dangerous for the riser since they result in very high bending stress in the riser, which might even exceed the yield stress. A necessary condition for the local dynamic buckling is that the riser is statically unstable at the moment of the maximum set down of the platform.

Acknowledgements

This research is supported by the Technology Foundation STW, applied science division of NWO and the technology programme of the Dutch Ministry of Economic Affairs.

References

[1] C.S. Hsu, The response of a parametrically excited hanging string in fluid, *Journal of Sound and Vibration* 39 (1975) 305–316.
[2] M.H. Patel, H.I. Park, Dynamics of tension leg platform tethers at low tension. Part I—Mathieu stability at large parameters, *Marine Structures* 4 (1991) 257–273.
[3] M.H. Patel, H.I. Park, Combined axial and lateral responses of tensioned buoyant platform tethers, *Engineering Structures* 17 (1995) 687–695.
[4] I.K. Chatjigeorgiou, S.A. Mavrakos, Bounded and unbounded coupled transverse response of parametrically excited vertical marine risers and tensioned cable legs for marine applications, *Applied Ocean Research* 24 (2002) 341–354.
[5] H. Suzuki, K. Takano, K. Enomoto, N. Oka, Axial and lateral response of a deepsea riser for scientific drilling, *Proceedings of Twenty Third International Conference on Offshore Mechanics and Arctic Engineering*, Vancouver, British Columbia, Canada, 2004 (OMAE2004-51094).
[6] I.K. Chatjigeorgiou, S.A. Mavrakos, Nonlinear resonances of parametrically excited risers—numerical and analytical investigation for $\Omega = 2\omega_1$, *Computers and Structures* 83 (2005) 560–573.
[7] H.I. Park, D.H. Jung, A finite element method for dynamic analysis of long slender marine structures under combined parametric and forcing excitations, *Ocean Engineering* 29 (2002) 1313–1325.
[8] G.L. Kuiper, A.V. Metrikine, J.A. Battjes, A new time-domain drag description and its influence on the dynamic behaviour of a cantilever pipe conveying fluid, *Journal of Fluids and Structures* 23 (2007) 429–445.
[9] A.H. Nayfeh, D.T. Mook, *Nonlinear Oscillations*, Wiley, New York, 1970.
[10] M.P. Païdoussis, *Fluid–Structure Interactions: Slender Structures and Axial Flow*, Vol. 1, Academic Press, London, 1998.
[11] G.L. Kuiper, A.V. Metrikine, Dynamic stability of a submerged, free-hanging riser conveying fluid, *Journal of Sound and Vibration* 280 (2005) 1051–1065.
[12] G. Floquet, Sur les équations différentielles linéaires à coefficients périodiques, *Annales scientifiques de l'École Normale Supérieure Sér. 2* 12 (1883) 47–88.